Catalysis Letters
https://doi.org/10.1007/s10562-020-03212-0

Synthesis of Pt@MAF-6 as a Steric Effect Catalyst for Selective Hydrogenation of Cinnamaldehyde

Kaizhen Xue[1] · Xiaocheng Lan[1] · Jinfu Wang[1] · Tiefeng Wang[1]

Received: 20 January 2020 / Accepted: 6 April 2020

Abstract

Pt@MAF-6 was designed as a highly selective catalyst for cinnamaldehyde hydrogenation. The aperture of Pt@MAF-6 acted to sterically confine cinnamaldehyde, and 94% selectivity to cinnamic alcohol was obtained at a high conversion of 95%. Steric confinement was inefficient in trans-2-pentenal hydrogenation, showing that encapsulating active sites within a commensurate porous support is important for a steric effect catalyst.

Graphic Abstract

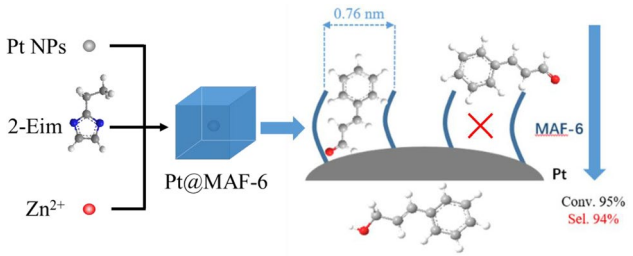

Keywords Steric effect · Unsaturated aldehyde · Metal-organic framework · Catalyst design · Selective hydrogenation

1 Introduction

Metal-organic frameworks (MOFs) are widely investigated for many applications, such as gas/liquid storage and separation [1], chemical sensor [2], drug delivery [3] and heterogeneous catalysis [4–7]. In particular, MOFs that encapsulate metal nanoparticles (NPs) are excellent catalysts for heterogeneous reactions [4], where MOFs serve as supports and help prevent the agglomeration of metal NPs during catalytic reactions. In addition, the well-defined porous structure of a MOF can impart a steric effect to the catalyst, and control its selectivity to different molecules. For example, Zhang et al. [8] encapsulated Pt NPs inside UIO-66, and showed that it gave shape selective properties in olefin hydrogenation. Furthermore, being comprised of unsaturated metal ions and functional groups on the organic linkers, MOFs themselves can be co-catalysts that work together with the metal NPs. For example, Chen et al. [9] developed ultrafine PdAg alloy NPs (~1.5 nm) in MIL-101 as a cascade reaction catalyst, which gave good catalytic activity and selectivity in the synthesis of 2-(4-aminophenyl)-1H-benzimidazole due to MOF Lewis acidity and synergy with the PdAg NPs.

Selective hydrogenation of unsaturated aldehydes to unsaturated alcohols is an important process in the chemical industry [10–15]. It is challenging to get a high selectivity to unsaturated alcohols because the hydrogenation of C=C is thermodynamically more favorable than that of C=O [16]. Several strategies have been used to design highly selective catalysts for the hydrogenation of unsaturated alcohols,

Electronic supplementary material The online version of this article (https://doi.org/10.1007/s10562-020-03212-0) contains supplementary material, which is available to authorized users.

✉ Tiefeng Wang
wangtf@tsinghua.edu.cn

[1] Beijing Key Laboratory of Green Reaction Engineering and Technology, Department of Chemical Engineering, Tsinghua University, Beijing 100084, China

Published online: 24 April 2020

including using the electronic effect [17–23], synergistic effect [24, 25], and steric effect [26–28]. In particular, the steric effect can be used to significantly enhance C = O hydrogenation selectivity. The mechanism is that the C = C bond is blocked by its substituents and steric confinement in the catalyst, while the tail-end C = O bond adsorb on the metal sites. For example, the pore size of zeolite Y (0.72 nm) is commensurate with the molecular size of cinnamaldehyde (0.54 × 0.92 nm), thus cinnamaldehyde was oriented to adsorb on Pt active sites through the C = O bond [29]. In our previous work [27], ZIF-8 with a aperture size of 0.42 nm was used to design a steric effect catalyst (Pt@ZIF-8) for the hydrogenation of 3-methylcrotonaldehyde. The selectivity to unsaturated alcohol was enhanced to 84% even at a high conversion of 90%. The steric effect requires a good fit of the pore size with the reactant molecule, so it is significant to develop a steric effect catalyst with an appropriate porous material for the selective hydrogenation of a specific unsaturated aldehyde.

MAF-6, comprised of Zn^{2+} and 2-ethylimidazole, is a MOF with a larger aperture size (7.6 Å) than ZIF-8 because of its longer imidazole ligand [30, 31]. The molecular size of cinnamaldehyde (5.4 × 9.2 Å) is a good fit with the aperture of MAF-6. Thus, we seek to develop a steric catalyst using MAF-6 for the steric confinement for the selective hydrogenation of cinnamaldehyde. The strategy of "bottle-around-a-ship" was used to encapsulated the metal active sites inside MAF-6. Although several MOFs, such as ZIF-8 and UIO-66, have been used to successfully encapsulate NPs by this strategy, it is still a challenge to encapsulate well the NPs in a particular MOF [7, 32]. Encapsulating NPs inside MAF-6 has not been investigated before. In addition, preparing Pt@MAF-6 with high purity is important for inhibiting the adsorption of the C = C bond. In this work, the synthesis of Pt@MAF-6 was investigated. The characterization results indicated that Pt NPs acted as the seeds for the growth of Pt@MAF-6 which resulted in smaller Pt@MAF-6 size with increasing Pt loading. The steric effect catalyst (Pt@MAF-6) was used for the selective hydrogenation of cinnamaldehyde, and a 94% selectivity to cinnamic alcohol (COL) was obtained even at a high conversion of 95%.

2 Experimental

2.1 Chemicals

NaOH, methanol, ethanol and acetone (Beijing Chemical Reagent), ethylene glycol, n-hexane, cyclohexane, ZnO and concentrated aqueous ammonia solution (25%) (General Reagent), $H_2PtCl_6{\cdot}6H_2O$, trans-2-pentenal and cinnamaldehyde (Sinopharm Chemical), 2-ethylimidazole (Eim) (TCI Shanghai) and polyvinylpyrrolidone (PVP, MW ≈ 58 000) were purchased and used without further purification.

2.2 Catalyst Preparation

2.2.1 Preparation of PVP-Stabilized Pt NPs

Pt NPs were prepared by a method modified from one in the literature [27, 33]. Typically, 60 mg (1.5 mmol) NaOH, 45.3 mg (0.0875 mmol) $H_2PtCl_6{\cdot}6H_2O$ and 100 mg PVP were mixed in 10 mL of ethylene glycol (EG) at room temperature in a 25 mL round-bottom flask. The solution was heated to 150 °C with vigorous stirring and kept at this temperature for 3 h to form a uniform black Pt/EG solution. The Pt NPs were collected from the Pt/EG solution by centrifugation after the addition of acetone. The obtained Pt NPs were washed three times with ethanol and hexane, collected by centrifugation and finally dispersed in 10 mL methanol.

2.2.2 Preparation of Pt@MAF-6

The Pt@MAF-6 was prepared by a "bottle around a ship" strategy. Typically, 0.814 g ZnO (10 mmol) was dissolved in aqueous ammonia solution (25%, 200 mL) as solution A, and 1.92 g Eim (20 mmol) premixed with 15 mL cyclohexane and Pt NPs were dissolved in 150 mL methanol as solution B. Solution A was dropped into solution B within 3–5 min with vigorous stirring at room temperature, and the mixed solution was kept stirred for 0.5 h. The product was collected by centrifugation and washed with methanol three times and finally dried at 40 °C in vacuum for 24 h.

2.2.3 Preparation of MAF-32, MAF-5 and MAF-6

The MAFs were synthesized using methods in the literature [30]. For MAF-32, 1.92 g Eim (20 mmol) was dissolved in 30 mL methanol as solution A, and 0.814 g ZnO (10 mmol) was dissolved in 25% aqueous ammonia solution (200 mL) as solution B. For MAF-5, 1.92 g Eim (20 mmol) was dissolved in 30 mL methanol as solution A, and 0.814 g ZnO (10 mmol) premixed with 6.5 mL cyclohexane was dissolved in 25% aqueous ammonia solution (200 mL) as solution B. For MAF-6, 0.814 g ZnO (10 mmol) was dissolved in 25% aqueous ammonia solution (200 mL) as solution A, and 1.92 g Eim (20 mmol) premixed with 15 mL cyclohexane was dissolved in 150 mL methanol as solution B. To synthesize the MAFs, solution A was dropped into solution B within 3–5 min under vigorous stirring at room temperature and the mixed solution was kept stirred for 0.5 h. The product was collected by centrifugation and washed with methanol three times and finally dried at 40 °C in vacuum for 24 h.

2.2.4 Preparation of Pt/MAF-6

To prepare Pt/MAF-6, 0.5 g MAF-6 was mixed with Pt NPs/methanol solution, followed by ultrasonic treatment for 1 h. The obtained sample was dried at room temperature for 24 h and was further dried at 60 °C for 5 h. The sample was reduced by hydrogen at 150 °C for 3 h prior to use.

2.3 Catalyst Characterization

Power X-ray diffraction (XRD) patterns were obtained by a Bruker Advance D8 X-ray diffractometer using Cu Kα monochromatic radiation (40 kV, 40 mA, λ = 1.5406 Å). The actual loading of Pt NPs on Pt@MAF-6 s and Pt@MAF-5 was measured by inductively coupled plasma (ICP, SPECTRO ARCOS) analysis. SEM images were obtained by a scanning electron microscope (JSM-7401F), and TEM images were obtained by a transmission electron microscope (JEM 2010) operated at 120 kV. The elemental mapping of the catalyst was obtained by a high angle annular dark field scanning transmission electron microscope (HAADF-STEM, FEI Titan Cubed G2300) operated at 300 kV. The Brunauer–Emmett–Teller (BET, Autosorb-iQ2-C) specific surface area was determined by Ar adsorption measurement at 87 K. Before analysis, the sample was evacuated under vacuum at 30 °C for 10 h. The thermal stability of the catalyst was studied by thermogravimetric analysis (TGA/DSC1/1600LF), where the sample was heated from 30 °C to 750 °C at a heating rate of 10 °C/min.

2.4 Hydrogenation Reaction

The hydrogenation reaction of cinnamaldehyde (CAL) and trans-2-pentenal was carried out at 80 °C and 3 MPa hydrogen pressure in an autoclave reactor. For the hydrogenation of CAL, 0.35 g catalyst, 30 mL ethanol, 0.2 g o-xylene (internal standard) and 0.75 g (5.67 mmol) CAL were used. For the hydrogenation of trans-2-pentenal, 0.35 g catalyst, 30 mL cyclohexane, 0.2 g n-hexanol (internal standard) and 0.477 g (5.67 mmol) trans-2-pentenal were used. After purging with hydrogen, the autoclave was pressurized with hydrogen to 3 Mpa and stirred at 800 r/min. The products were analyzed with a gas chromatograph (GC 7900II) equipped with a FFAP capillary column (30 m × 0.32 mm × 0.5 μm) and a flame ionization detector. The response factors of the species were determined with standard samples.

The conversion was calculated as:

$$\text{Conversion}\ (\%) = \frac{N_{A,0} - N_{A,t}}{N_{A,0}} \times 100\%, \quad (1)$$

where $N_{A,0}$ was the initial mole of reactant, and $N_{A,t}$ was mole of reactant after reaction.

The selectivity was calculated as:

$$\text{Selectivity}\ (\%) = \frac{N_{COL,t}}{N_{COL,t} + N_{HCAL,t} + N_{HCOL,t}} \times 100\%, \quad (2)$$

where $N_{COL,t}$, $N_{HCAL,t}$ and $N_{HCOL,t}$ were the moles of cinnamic alcohol (COL), hydride cinnamaldehyde (HCAL) and hydride cinnamic alcohol (HCOL) after reaction, respectively.

3 Results and Discussion

3.1 Catalyst Synthesis and Characterization

There are several MAF isomers, such as MAF-32, MAF-5 and MAF-6, which have different topologies and pore sizes. The preparation of MAF-6 with high purity is important for fabricating the steric effect catalyst for the hydrogenation of CAL. He et al. [30] reported that the crystallization of Zn(II) 2-ethylimidazolate isomers can be controlled by varying the template, feeding order and reactant concentration. Herein, we further investigated the effect of template and feeding order on the crystal phases in order to prepare pure MAFs as the catalyst support.

The XRD patterns in Fig. S1 indicated that pure MAF-32 was obtained when no template was used. With increasing template concentration, the obtained sample changed from pure MAF-32, mixture of MAF-32 and MAF-5 to pure MAF-5 (Table S1.1–4). A high template concentration in methanol and the feeding order were crucial to get pure MAF-6 (Table S1.5–7). TEM and SEM images (Fig. S2) indicated that the obtained pure MAF-6 had a uniform polyhedron shape, while MAF-5 exhibited a wide range of particle sizes (2–10 μm). MAF-32 exhibited an amorphous structure and a nonuniform particle size. These samples had different surface areas and pore volumes. As shown in Table 1, the BET surface area and pore volume decreased as follows: MAF-6 (1623 m^2/g, 0.67 cm^3/g) > MAF-5 (481 m^2/g, 0.27 cm^3/g) > MAF-32 (12 m^2/g, 0.034 cm^3/g). Since a low surface area and pore volume are unbeneficial for encapsulating Pt NPs [5, 7], the formation of MAF-5 and MAF-32 isomers should be avoided during the preparing of Pt@MAF-6.

The Pt@MAF-6 catalysts with different metal loadings of Pt were prepared by a "bottle around a ship" approach. Pt NPs with a mean particle size of 1.7 nm (Fig. S3) were dispersed in the methanol solvent of the organic ligand precursor. Based on the results of the blank MAFs preparation, the same amount of template was added into the methanol solvent to get the MAF-6 crystal phase. The Pt loading of

Table 1 Catalyst characterization

Entry	Sample	D[b], nm	S_{BET}, m^2/g	V_{total}[c], cm^3/g	D_{pore}[c], nm
1	1.61%Pt@MAF-6[a]	461	1339	0.64	1.91
2	0.76%Pt@MAF-6[a]	500	1538	0.67	1.91
3	0.30%Pt@MAF-6[a]	678	1561	0.64	1.91
4	MAF-6	733	1623	0.67	1.91
5	0.21%Pt@MAF-5[a]	–	445	0.19	1.36
6	MAF-5	–	481	0.27	1.40
7	MAF-32	–	12	0.034	50.23

[a]Metal loading determined by ICP analysis, [b]D is the average diameter of the samples measured from TEM images

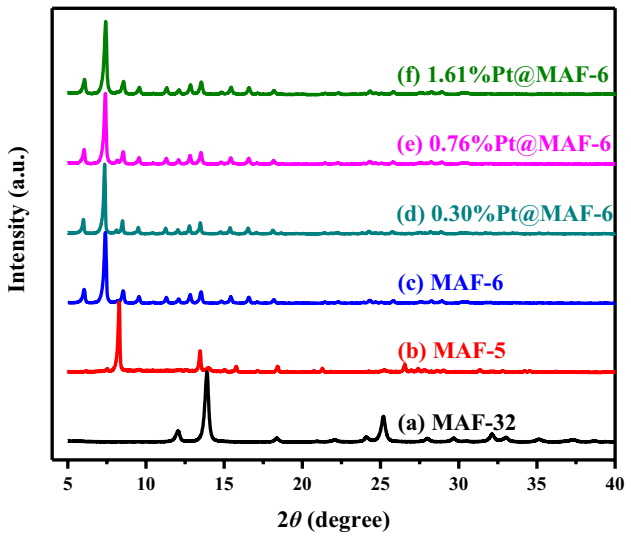

Fig. 1 XRD profiles of **a** MAF-32, **b** MAF-5, **c** MAF-6, **d** 0.30%Pt@MAF-6, **e** 0.76%Pt@MAF-6, and **f** 1.61%Pt@MAF-6

Pt@MAF-6 was determined by ICP analysis and the catalysts were denoted as *x*% Pt@MAF-6, where *x* was the Pt loading. XRD results (Fig. 1) demonstrated that all the Pt@MAF-6 catalysts have the diffraction pattern of MAF-6. The morphology and structure of Pt@MAF-6 were determined by SEM and TEM characterizations. As shown in Fig. 2, these catalysts exhibited a uniform polyhedron structure. Interestingly, a Pt loading dependence of the crystal size was obtained with the Pt@MAF-6 catalysts. The crystal size of Pt@MAF-6 decreased with increasing Pt loading, with 461, 500, and 678 nm Pt@MAF-6 catalysts (Fig. S4) obtained at metal loadings of 1.61%, 0.76% and 0.30%, respectively. It was reported that the crystal size of the MOF was determined by the nucleation and growth processes and a fast nucleation gave a small crystal size [34, 35]. MAF-6 exhibited a lower rate of nucleation than growth under the present condition, thus a large crystal size of 733 nm was obtained for the blank MAF-6. With the addition of Pt NPs, the metal ligand of MAF-6 bonded with the NPs and further acted as the seeds for the next growth, which thus decreased the crystal size. These results also indicated that the Pt NPs were encapsulated inside MAF-6 during the growth process.

HAADF-STEM images and EDS elemental mapping images of 0.30%Pt@MAF-6 (Fig. 3), 0.3%Pt/MAF-6 and MAF-6 (Fig. S5) were used to further determine the Pt NPs distribution, and showed that Pt NPs of 1.7 nm were uniformly encapsulated inside MAF-6 (Fig. 3c). The lattice spacing of the Pt NPs in 0.30%Pt@MAF-6 was determined as 0.22 nm (Fig. 3d), which corresponded to the Pt (111) crystal plane. The well-dispersed red bright spots in the EDS elemental mapping of 0.30%Pt@MAF-6 (Fig. 3e–h) were ascribed to Pt NPs. For 0.30%Pt@MAF-6, most of the Pt NPs were evenly distributed inside MAF-6. With increased Pt loading, some Pt NPs were distributed near the outer surface of MAF-6 (Fig. S6), and some aggregated Pt NPs were observed.

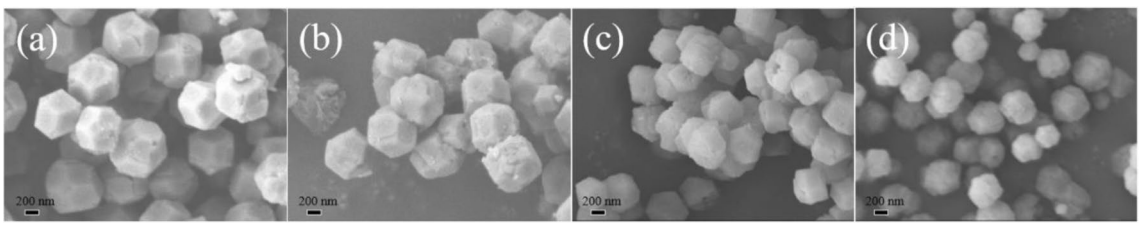

Fig. 2 SEM images of **a** MAF-6, **b** 0.3%Pt@MAF-6, **c** 0.76%Pt@MAF-6, **d** 1.61%Pt@MAF-6

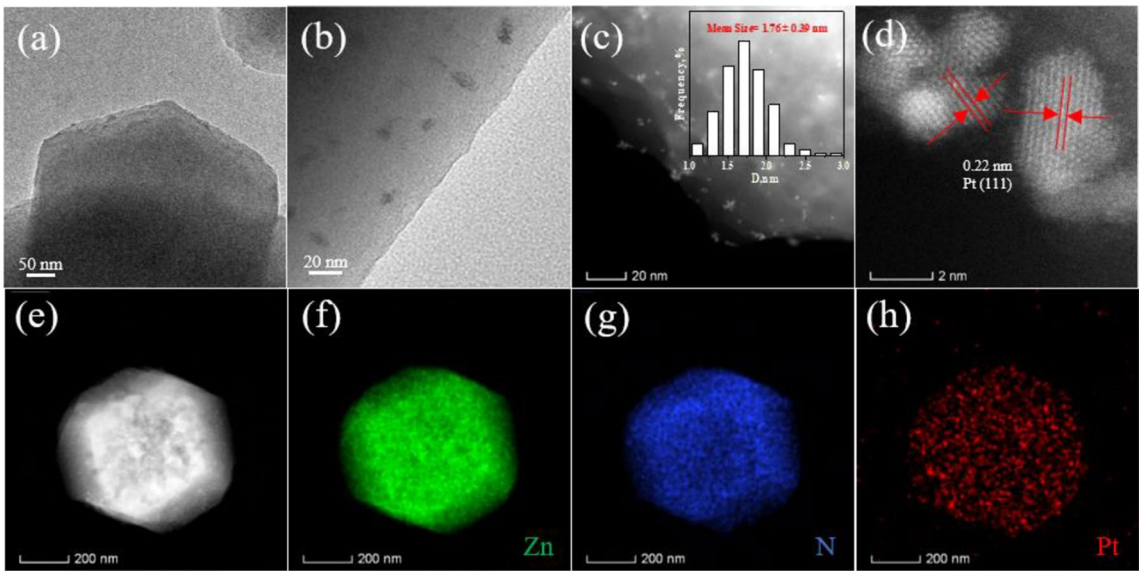

Fig. 3 Nanostructure of 0.3%Pt@MAF-6. **a**, **b** TEM images, **c** HAADF-STEM image and histogram of Pt NP size distribution, **d** Pt (111) lattice fringe image, **e**–**h** EDS elemental mapping images

Pt NPs were also supported on the external surface of MAF-6 (Pt/MAF-6) and encapsulated in MAF-5 (Pt@MAF-5) for comparison. For 0.3%Pt/MAF-6 and 1.61%Pt/MAF-6 (Fig. S7), the impregnation process did not affect the structure of MAF-6. The Pt NPs were supported on the external surface of MAF-6 because their particle size was larger than the aperture of MAF-6. With increasing Pt loading, some Pt NPs agglomerated to larger particles due to the small external surface of MAF-6. HRTEM images of the fringes of the Pt/MAF-6 and Pt@MAF-6 were showed in Fig. S8. For the Pt/MAF-6 catalyst, Pt NPs were supported on the surface of MAF-6 after the blank MAF-6 was synthesized. Obviously, Pt NPs were distributed on the surface and some Pt NPs were located at the fringes of MAF-6. Compared with Pt/MAF-6, no Pt NPs were distributed in the fringes of Pt@MAF-6. For Pt@MAF-5, Ar adsorption results (Table 1) indicated that MAF-5 exhibited a much smaller surface area than MAF-6 and the smaller surface area was unbeneficial for good dispersion and encapsulation of Pt NPs. In addition, some amorphous structure was obtained with the Pt@MAF-5 catalysts (Fig. S9).

The pore structure of Pt@MAF-6 was determined by Ar adsorption (Table 1 & Fig. 4). The BET surface areas of the Pt@MAF-6 catalysts were slightly smaller than that

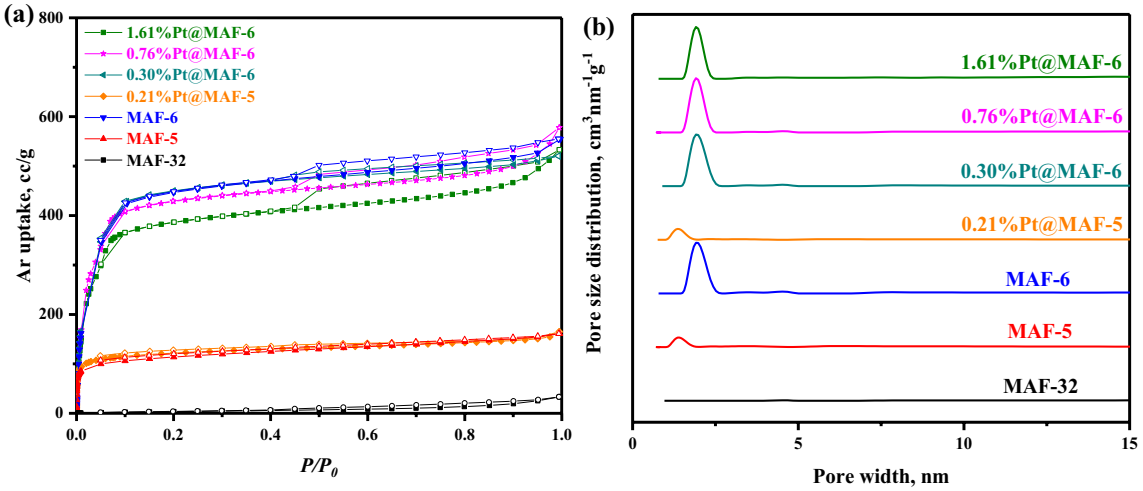

Fig. 4 **a** Ar adsorption isotherms at 87 K and **b** pore size distribution of MAF-32, MAF-5, MAF-6, Pt@MAF-5, and Pt@MAF-6

of MAF-6 and showed a negative correlation with Pt loading, which was because of the Pt NPs encapsulated in the inner space of MAF-6. The pore size distributions of these samples are shown in Fig. 4b. All the Pt@MAF-6 catalysts exhibited an identical pore size distribution as the blank MAF-6, indicating that the incorporation of Pt NPs into MAF-6 did not change the pore structure of MAF-6. In addition, thermogravimetric analysis (Fig. S10) showed that the Pt@MAF-6 catalysts preserved the good thermal stability of blank MAF-6.

3.2 Hydrogenation Reaction

The results of the selective hydrogenation of CAL are listed in Table 2. It has been reported that the C = C bond hydrogenation is thermally favored over that of C = O, thus the intrinsic COL selectivity over Pt metal was low. Only 33% selectivity to COL was obtained over the Pt/C catalyst [10]. Here, unsupported PVP-Pt NPs were investigated for comparison in the hydrogenation of CAL. As listed in Table 2, PVP-Pt NPs gave a COL selectivity of 54.4% at a CAL conversion of 75.6%, which was higher than that of the Pt/C catalyst reported in previous work. The higher selectivity over the PVP-Pt NPs was ascribed to a steric effect induced by modifying the metal NPs with PVP ligand [36]. The selectivity to COL was significantly enhanced by encapsulating the Pt NPs inside MAF-6. As listed in Table 2, a much higher selectivity to COL (> 94%) was obtained over Pt@MAF-6. For a better comparison, the selectivity to COL was plotted as a function of CAL conversion (Fig. 5). The results showed that the Pt@MAF-6 catalyst exhibited a much higher selectivity to COL than Pt NPs, which was attributed to the steric effect of the MAF-6 aperture.

The catalyst characterization results revealed that Pt NPs acted as seeds for the growth of MAF-6 and were encapsulated inside the MAF-6 crystal. The Pt signal was well dispersed over the MAF-6 crystal (Fig. 3g), and the XRD and Ar adsorption results demonstrated that Pt@MAF-6 kept the

Table 2 Selective hydrogenation of cinnamaldehyde and trans-2-pentenal by different catalysts

Reaction

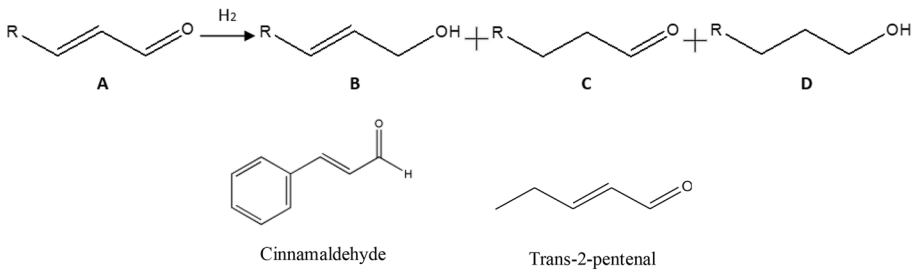

Entry	Catalysts	Time (h)	Conversion (%)	Selectivity (%)			
				B	C	D	Other
Cinnamaldehyde							
1	0.30%Pt@MAF-6	48	47.1	94.7	3.5	1.0	0.9
2	0.76%Pt@MAF-6	48	81.5	95.3	2.2	1.9	0.6
3	1.61%Pt@MAF-6	48	95.2	94.0	3.2	1.8	0.9
4	0.30%Pt/MAF-6	48	14.3	82.5	11.6	0.7	5.2
5	1.61%Pt/MAF-6	48	62.8	89.4	7.5	1.1	2.0
6	0.21%Pt@MAF-5	48	32.0	83.2	11.6	2.8	2.4
7	PVP-Pt NPs[a]	24	75.6	54.4	40.6	0.1	5.0
Trans-2-pentenal							
8	0.30%Pt@MAF-6	24	9.9	47.4	41.3	11.3	-
9	0.30%Pt/MAF-6	24	5.8	65.9	27.7	6.4	-

Reaction condition: 0.35 g catalysts with Pt NPs; the reaction used 5.67 mmol of A at 80 °C and 3 MPa H_2

Solvent and internal standard for the cinnamaldehyde reaction: 30 mL ethanol, 0.2 g o-xylene

Solvent and internal standard for the trans-2-pentenal reaction: 30 mL cyclohexane, 0.2 g n-hexanol

[a]1.05 mg Pt NPs consistent with 0.3%Pt@MAF-6 used in the reaction

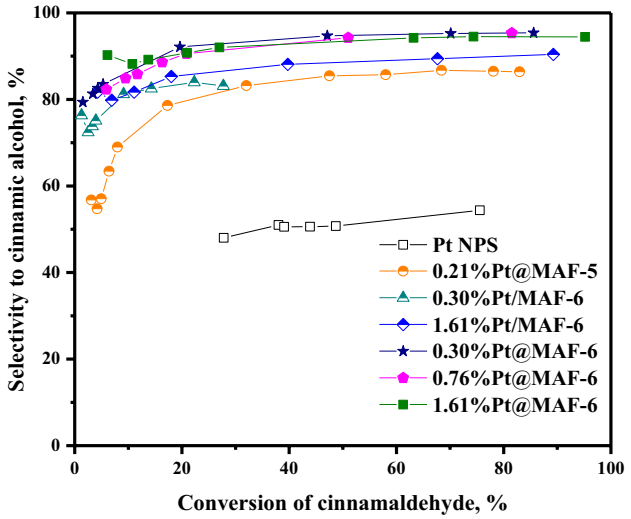

Fig. 5 Comparison of conversion-selectivity relationship over Pt NPs, 0.21%Pt@MAF-5, 0.3%Pt/MAF-6, 1.61%Pt/MAF-6, 0.30%Pt@MAF-6, 0.76%Pt@MAF-6, 1.61%Pt@MAF-6. Conversion and selectivity data were gathered from Fig. S11

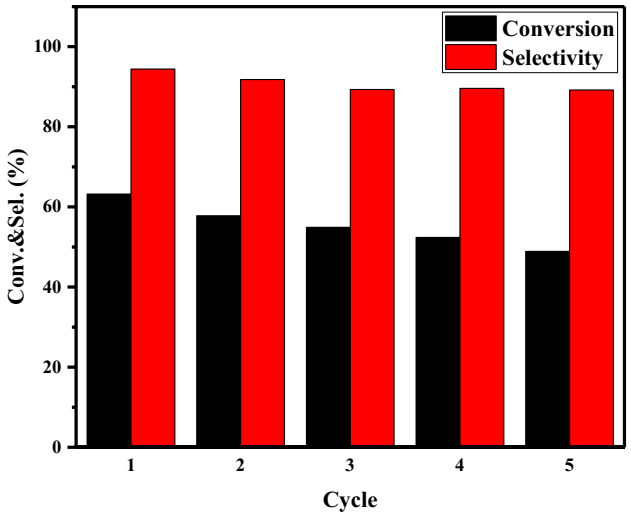

Fig. 6 Recycle experiment of selective hydrogenation of cinnamaldehyde. Reaction conditions: 0.35 g catalyst, 5.67 mmol cinnamaldehyde, 0.2 g o-xylene, 30 mL ethanol at 80 °C and 3 MPa H_2, reaction time of 24 h

structure and pore structure of MAF-6. These results indicated that the Pt active sites of Pt@MAF-6 were modified by the aperture of MAF-6, which generated a confinement shell for the adsorbed CAL molecules. The molecular size of CAL (5.4×9.4 Å) is commensurate with the aperture size of MAF-6 (7.6 Å). The steric effect between the aperture and the phenyl group of CAL led to perpendicular adsorption of CAL on the active sites by the C=O bond while preventing the adsorption of the C=C bond. Thus, a much higher selectivity to COL was obtained over Pt@MAF-6 even at a high conversion of 85%.

The selective hydrogenation of CAL was also investigated over Pt/MAF-6 and Pt@MAF-5, which showed a lower selectivity to COL than Pt@MAF-6. The selectivity was 82.5%, 89.4% and 83.2% over 0.3%Pt/MAF-6, 1.61%Pt/MAF-6 and 0.21%Pt@MAF-5, respectively. However, the selectivity of these catalysts was still higher than that of unsupported Pt NPs. The enhanced selectivity over the Pt/MAF-6 catalysts was due to two reasons: one was the electronic modification of the MAF-6 support of the Pt NPs and the other was the agglomeration of Pt NPs on the external surface of MAF-6. Pt NPs prepared by liquid phase reduction have a particle size of 1.7 nm, which was larger than the aperture size of MAF-6, thus the Pt NPs were supported on the external surface of MAF-6. The TEM images showed that the crystal size of blank MAF-6 was 732 nm (Fig. S4a). The small external surface area was unbeneficial for the high dispersion of Pt NPs, thus some agglomerated Pt NPs were obtained over Pt/MAF-6 (Fig. S8). This was consistent with the reaction results that Pt/MAF-6 had a much lower reaction activity than Pt@MAF-6 (Table 2), where the conversion decreased to 14.3% and 62.8% over 0.30%Pt/MAF-6 and 1.61%Pt/MAF-6, respectively. It was reported that the selectivity to COL showed a size dependence on the metal particles and larger particles gave a higher selectivity to COL [10, 22, 37]. Thus, the selectivity to COL over Pt/MAF-6 could be enhanced by the agglomeration of Pt NPs. The enhanced selectivity induced by Pt particle size was also verified over the Pt/SiO_2 catalyst (Fig. S11h). Pt/SiO_2 prepared by impregnation method showed a mean particle size of 2.85 nm (Fig. S12), which was larger than the unsupported Pt NPs. Thus, the selectivity to cinnamic alcohol over Pt/SiO_2 (78%) was higher than that over unsupported Pt NPs (54%). For the Pt@MAF-5 catalyst, the BET surface area of MAF-5 (481 m^2/g) was much lower than MAF-6 (1623 m^2/g). The lower surface area was unbeneficial for good dispersion and encapsulation of Pt NPs. In addition, some amorphous structure was obtained with the Pt@MAF-5 catalysts (Fig. S9). Thus, although the aperture size of MAF-5 (4.0×5.8 Å) was commensurate with CAL, Pt@MAF-5 showed lower activity and selectivity to COL than Pt@MAF-6.

The recycle experiment of 1.61%Pt@MAF-6 for the hydrogenation of cinnamaldehyde was carried out and the results are shown in Fig. 6. After reaction, the catalyst was separated by centrifugation and reused for the next run without any washing or reactivation steps. As shown in Fig. 6, > 90% selectivity to unsaturated alcohol was obtained for each reaction and the conversion decreased from 63% to 49%. The spent catalyst was characterized by TEM (Fig. S13) indicating that the catalyst kept its crystallization structure. The decrease in activity could be ascribed to the loss

of catalyst during the reusing process and the deactivation by product deposition [38–40].

The Pt@MAF-6 catalyst was further investigated for the selective hydrogenation of trans-2-pentenal (Fig. S14). In contrast to the hydrogenation of CAL, the 0.30%Pt/MAF-6 catalyst (65.9%) showed a higher selectivity to unsaturated alcohol than the Pt@MAF-6 catalyst (47.4%). The small external surface area of MAF-6 was unbeneficial for the high dispersion of Pt NPs, thus some agglomerated Pt NPs were obtained over Pt/MAF-6 (Fig. S8). It has been well documented that larger metal particles exhibited a higher selectivity to unsaturated alcohol due to the particle size effect [10, 22, 37]. Moreover, the steric confinement was inefficient for controlling the correct adsorption mode of 2-pentenal on the active sites of Pt@MAF-6, because the molecular size of 2-pentenal is 0.40×0.81 nm, which is smaller than the aperture size of MAF-6. Thus, Pt/MAF-6 showed a higher selectivity to unsaturated alcohol than Pt@MAF-6. These results indicated that encapsulating active sites with a commensurate porous support is important for designing a steric effect catalyst.

4 Conclusions

We developed a steric effect catalyst (Pt@MAF-6) for the selective hydrogenation of CAL. XRD, SEM, and HAADF-STEM characterization were used to determine the morphology, structure, and Pt NPs distribution of Pt@MAF-6. The characterization results also indicated that Pt NPs acted as the seeds for the growth of Pt@MAF-6 which resulted in decreased Pt@MAF-6 size with increasing Pt loading. Pt@MAF-6 gave 94% selectivity to cinnamic alcohol (COL) even at a high conversion of 95%. This high selectivity was ascribed to the steric confinement by the MAF-6 aperture of the CAL adsorption mode. The steric confinement was inefficient for the smaller molecule of trans-2-pentenal, showing that a good fit with the porous material is important for designing a steric effect catalyst.

Acknowledgement This work was supported by the National Natural Science Foundation of China (no. 21676155), PetroChina Innovation Foundation (2016D-5007–0507), China Postdoctoral Science Foundation (2019M660660), and Shuimu Tsinghua Scholar program.

References

1. Li JR, Sculley J, Zhou HC (2012) Metal–organic frameworks for separations. Chem Rev 112:869–932
2. Kreno LE, Leong K, Farha OK, Allendorf M, Van Duyne RP, Hupp JT (2012) Metal–organic framework materials as chemical sensors. Chem Rev 112:1105–1125
3. Huxford RC, Della Rocca J, Lin W (2010) Metal–organic frameworks as potential drug carriers. Curr Opin Chem Biol 14:262–268
4. Zhao S-N, Song X-Z, Song S-Y, Zhang H-J (2017) Highly efficient heterogeneous catalytic materials derived from metal-organic framework supports/precursors. Coordin Chem Rev 337:80–96
5. Yang Q, Xu Q, Jiang HL (2017) Metal–organic frameworks meet metal nanoparticles: synergistic effect for enhanced catalysis. Chem Soc Rev 46:4774–4808
6. Liu J, Chen L, Cui H, Zhang J, Zhang L, Su CY (2014) Applications of metal–organic frameworks in heterogeneous supramolecular catalysis. Chem Soc Rev 43:6011–6061
7. Hu P, Morabito JV, Tsung C-K (2014) Core–shell catalysts of metal nanoparticle core and metal–organic framework shell. ACS Catal 4:4409–4419
8. Zhang W, Lu G, Cui C, Liu Y, Li S et al (2014) A family of metal-organic frameworks exhibiting size-selective catalysis with encapsulated noble-metal nanoparticles. Adv Mater 26:4056–4060
9. Chen Y-Z, Zhou Y-X, Wang H, Lu J, Uchida T et al (2015) Multifunctional PdAg@ MIL-101 for one-pot cascade reactions: combination of host–guest cooperation and bimetallic synergy in catalysis. ACS Catal 5:2062–2069
10. Gallezot P, Richard D (1998) Selective hydrogenation of α, β-unsaturated aldehydes. Catal Rev 40:81–126
11. Kliewer CJ, Bieri M, Somorjai GA (2009) Hydrogenation of the α, β-unsaturated aldehydes acrolein, crotonaldehyde, and prenal over Pt single crystals: a kinetic and sum-frequency generation vibrational spectroscopy study. J Am Chem Soc 131:9958–9966
12. Kennedy G, Baker LR, Somorjai GA (2014) Selective Amplification of C=O bond hydrogenation on Pt/TiO2: catalytic reaction and sum-frequency generation vibrational spectroscopy studies of crotonaldehyde hydrogenation. Angew Chem Int Ed Engl 53:3405–3408
13. Mäki-Arvela P, Hájek J, Salmi T, Murzin DY (2005) Chemoselective hydrogenation of carbonyl compounds over heterogeneous catalysts. Appl Catal A-Gen 292:1–49
14. Tian Z, Xiang X, Xie L, Li F (2012) Liquid-phase hydrogenation of cinnamaldehyde: enhancing selectivity of supported gold catalysts by incorporation of cerium into the support. Ind Eng Chem Res 52:288–296
15. Lan X, Wang T (2020) Highly selective catalysts for the hydrogenation of unsaturated aldehydes: a review. ACS Catal 10:2764–2790
16. Ide MS, Hao B, Neurock M, Davis RJ (2012) Mechanistic insights on the hydrogenation of α, β-unsaturated ketones and aldehydes to unsaturated alcohols over metal catalysts. ACS Catal 2:671–683
17. Ammari F, Milone C, Touroude R (2005) Selective hydrogenation of crotonaldehyde on Pt/ZnCl2/SiO2 catalysts. J Catal 235:1–9
18. Durndell LJ, Parlett CMA, Hondow NS, Isaacs MA, Wilson K, Lee AF (2015) Selectivity control in Pt-catalyzed cinnamaldehyde hydrogenation. Sci Rep 5:9425
19. Merlo AB, Machado BF, Vetere V, Faria JL, Casella ML (2010) PtSn/SiO2 catalysts prepared by surface controlled reactions for the selective hydrogenation of cinnamaldehyde. Appl Catal A-Gen 383:43–49
20. Neri G, Arrigo I, Corigliano F, De Luca L, Donato A (2011) Selective hydrogenation of cinnamaldehyde on Pt and Pt-Fe catalysts supported on zeolite P. Catal Lett 141:1590–1597
21. Prakash MG, Mahalakshmy R, Krishnamurthy KR, Viswanathan B (2016) Studies on Ni–M (M= Cu, Ag, Au) bimetallic catalysts for selective hydrogenation of cinnamaldehyde. Catal Today 263:105–111
22. Prashar AK, Mayadevi S, Nandini Devi R (2012) Effect of particle size on selective hydrogenation of cinnamaldehyde by Pt encapsulated in mesoporous silica. Catal Commun 28:42–46

23. Zheng R, Porosoff MD, Weiner JL, Lu S, Zhu Y, Chen JG (2012) Controlling hydrogenation of C=O and C=C bonds in cinnamaldehyde using silica supported Co-Pt and Cu-Pt bimetallic catalysts. Appl Catal A 419–420:126–132
24. Lan X, Wang T, Li X, Huang N, Wang J (2016) Pt@SnOx/SiO_2 catalysts with enhanced selectivity to allyl alcohol for acrolein hydrogenation. Catal Sci Technol 6:7703–7707
25. Lan X, Xue K, Wang T (2019) Combined synergetic and steric effects for highly selective hydrogenation of unsaturated aldehyde. J Catal 372:49–60
26. Guo Z, Xiao C, Maligal-Ganesh RV, Zhou L, Goh TW et al (2014) Pt nanoclusters confined within metal–organic framework cavities for chemoselective cinnamaldehyde hydrogenation. ACS Catal 4:1340–1348
27. Lan X, Huang N, Wang J, Wang T (2017) Geometric effect in the highly selective hydrogenation of 3-methylcrotonaldehyde over Pt@ZIF-8 core–shell catalysts. Catal Sci Technol 7:2601–2608
28. Zhao M, Yuan K, Wang Y, Li G, Guo J et al (2016) Metal–organic frameworks as selectivity regulators for hydrogenation reactions. Nature 539:76–80
29. Gallezot P, Giroir-Fendler A, Richard D (1990) Chemioselectivity in cinnamaldehyde hydrogenation induced by shape selectivity effects in Pt-Y zeolite catalysts. Catal Lett 5:169
30. He CT, Jiang L, Ye ZM, Krishna R, Zhong ZS et al (2015) Exceptional hydrophobicity of a large-pore metal–organic zeolite. J Am Chem Soc 137:7217–7223
31. Bhadra BN, Seo PW, Khan NA, Jhung SH (2016) Hydrophobic cobalt-ethylimidazolate frameworks: phase-pure syntheses and possible application in cleaning of contaminated water. Inorg Chem 55:11362–11371
32. Meilikhov M, Yusenko K, Esken D, Turner S, Van Tendeloo G, Fischer RA (2010) Metals@MOFs—Loading MOFs with metal nanoparticles for hybrid functions. Eur J Inorg Chem 24:3701–3714
33. Teranishi T, Hosoe M, Tanaka T, Miyake M (1999) Size control of monodispersed Pt nanoparticles and their 2D organization by electrophoretic deposition. J Phys Chem B 103:3818–3827
34. Lu G, Li S, Guo Z, Farha OK, Hauser BG et al (2012) Imparting functionality to a metal–organic framework material by controlled nanoparticle encapsulation. Nat Chem 4:310–316
35. Lan X, Huang N, Wang J, Wang T (2018) A general and facile strategy for precisely controlling the crystal size of monodispersed metal–organic frameworks via separating the nucleation and growth. Chem Commun 54:584–587
36. Chen L, Zhan W, Fang H, Cao Z, Yuan C et al (2017) Selective catalytic performances of noble metal nanoparticle@ MOF composites: the concomitant effect of aperture size and structural flexibility of MOF matrices. Chemistry 23:11397–11403
37. Galvagno S, Capannelli G, Neri G, Donato A, Pietropaolo R (1991) Hydrogenation of cinnamaldehyde over Ru/C catalysts: effect of Ru particle size. J Mol Catal 64:237–246
38. Rudolf C, Dragoi B, Ungureanu A, Chirieac A, Royer S et al (2014) NiAl and CoAl materials derived from takovite-like LDHs and related structures as efficient chemoselective hydrogenation catalysts. Catal Sci Technol 4:179–189
39. Zheng Q, Wang D, Yuan F, Han Q, Dong Y, Liu Y et al (2016) An Effective Co-promoted platinum of Co–Pt/SBA-15 catalyst for selective hydrogenation of cinnamaldehyde to cinnamyl alcohol. Catal Lett 146:1535–1543
40. Wei S, Zhao Y, Fan G, Yang L, Li F (2017) Structure-dependent selective hydrogenation of cinnamaldehyde over high-surface-area CeO2-ZrO2 composites supported Pt nanoparticles. Chem Eng J 322:234–245